PNAS NEXUS

PNAS Nexus, 2025, 4, pgaf070
https://doi.org/10.1093/pnasnexus/pgaf070
Advance access publication 10 March 2025
Research Report

Methamphetamine alters the circadian oscillator and its couplings on multiple scales in *Per1/2/3* knockout mice

Samuel J.K. Barnes [a], Mansour Alanazi [a,b], Shin Yamazaki [c] and Aneta Stefanovska [a,*]

[a]Physics Department, Lancaster University, Lancaster LA1 4YB, United Kingdom
[b]Department of Physics, Northern Border University, Arar 73311, Kingdom of Saudi Arabia
[c]Department of Neuroscience and Peter O'Donnell Jr. Brain Institute, UT Southwestern Medical Center, Dallas, TX 75390-9111, USA
*To whom correspondence should be addressed: Email: aneta@lacaster.ac.uk
Edited By Daniel Aeschbach

Abstract

Disruptions to circadian rhythms in mammals are associated with alterations in their physiological and mental states. Circadian rhythms are currently analyzed in the time domain using approaches such as actograms, thus failing to appreciate their time-localized characteristics, time-varying nature and multiscale dynamics. In this study, we apply time-resolved analysis to investigate behavioral rhythms in *Per1/2/3* knockout (KO) mice and their changes following methamphetamine administration, focusing on circadian (around 24 h), low-frequency ultradian (around 7 h), high-frequency ultradian (around 30 min), and circabidian (around 48 h) oscillations. In the absence of methamphetamine, *Per1/2/3* KO mice in constant darkness exhibited a dominant, ∼7 h oscillation. We demonstrate that methamphetamine exposure restores the circadian rhythm, although the frequency of the methamphetamine sensitive circadian oscillator varied considerably compared to the highly regular wild-type circadian rhythm. Additionally, methamphetamine increased multiscale activity and induced a circabidian oscillation in the *Per1/2/3* KO mice. The information transfer between oscillatory modes, with frequencies around circadian, low-frequency ultradian and high-frequency ultradian activity, due to their mutual couplings, was also investigated. For *Per1/2/3* KO mice in constant darkness, the most prevalent coupling was between low and high-frequency ultradian activity. Following methamphetamine administration, the coupling between the circadian and high-frequency ultradian activity became dominant. In each case, the direction of information transfer was between the corresponding phases from the slower to faster oscillations. The time-varying nature of the circadian rhythm exhibited in the absence of *Per1/2/3* genes and following methamphetamine administration may have profound implications for health and disease.

Keywords: circadian rhythms, biological oscillators, time-resolved analysis, multiscale analysis, nonlinear dynamics

Significance Statement

Disrupted circadian rhythms are implicated in several pathologies. This study reveals the time-varying multiscale dynamics underlying such rhythms in mice. By analyzing the wheel running activity of mice lacking canonical circadian clocks (*Per1/2/3* KO) exposed to methamphetamine, which stimulates dopamine signaling, we demonstrate the dynamical characteristics of the methamphetamine sensitive circadian oscillator (MASCO). Although the MASCO period coincides with the canonical circadian rhythm, its frequency varies significantly in time. Methamphetamine administration also increased multiscale activity, induced a circabidian oscillation, and altered couplings between behavioral modes. The time-varying MASCO may explain the sleep-wake cycle disturbances reported in individuals treated with stimulants, especially those with attention-deficit/hyperactivity disorder (ADHD). This research highlights the importance of time-resolved analysis in revealing previously unexplored aspects of circadian biology.

Introduction

Periodic activity manifests across all temporal and spatial scales throughout nature. One of the most widely recognized cycles is the circadian rhythm, which is closely associated with numerous pathologies (1–3). In mammals, the circadian rhythm is primarily regulated by the suprachiasmatic nucleus (SCN) (4, 5), which serves as a central pacemaker entrained to the light/dark cycle (6). Additionally, peripheral oscillators are affected by nonphotic cues such as restricted feeding (7, 8) and methamphetamine administration (9, 10). However, the relationship between canonical circadian oscillators and those influenced by dietary or pharmacological interventions remains unclear.

Mammalian circadian rhythms are governed by transcriptional–translational feedback loops within cells (5, 11, 12). *Period* (*Per*) genes are known to regulate circadian behaviors (13). The removal of these genes disrupts the 24-h timekeeping system, thereby eliminating the circadian rhythm (14). Consequently, *Per1/2/3* knockout (KO) mice offer a model to explore alternative

Competing Interest: The authors declare no competing interests.
Received: October 4, 2024. **Accepted:** February 10, 2025

pacemakers such as the methamphetamine sensitive circadian oscillator (MASCO), which operates independently of canonical clock genes (15). This approach avoids the interference from endogenous canonical circadian oscillations that would otherwise confound the results.

In addition to circadian oscillations (~24 h) (16–21), ultradian (<24 h) (22) and infradian (>24 h) (23) rhythms coexist, resulting from several biological mechanisms. These range from cellular dynamics occurring over minutes (24) to elongated multiday periods (25). Current methods largely analyze behavioral rhythms in the time domain using techniques such as actograms (26). Recently introduced multiscale analysis methods (27–34), able to detect the presence of oscillations and their mutual interactions on wide time-scales, promise to advance the study of behavioral rhythms. Additionally, they explicitly consider time as a physical parameter (35, 36), enabling time-localization. Hence, they are not based on time-asymptotic assumptions and therefore enable the temporal variability of these oscillations to be explored. In contrast, traditional, time-asymptotic analysis approaches may inappropriately categorize deterministic oscillations acting on multiple scales with time-varying frequency as noise (33).

Although ultradian rhythms are ubiquitous in biological systems and are found in all organisms from single cells to complex multicellular animals, their origin is still unclear (22, 37, 38). There is no known environmental signal that synchronizes with ultradian rhythms (38). However, it has been shown that ultradian rhythms interact with the circadian rhythm and the daily light/dark cycle (39) and that ultradian rhythmicity can persist in the absence of functional molecular circadian clocks at both behavioral and cellular levels (40, 41). Recent study suggests that the balance between circadian and ultradian rhythmicity is determined by energy balance (42). It is also known that there are multiple ultradian rhythms of physiological or behavioral origin, and that they can be synchronized with each other. However, no central ultradian pacemaker has been identified so far (43). Yet, it has been shown that among the coupled ultradian rhythms, the hippocampal theta wave is phase leading, suggesting a central control of some of the ultradian rhythms (43). It has also been shown that striatal dopamine exhibits an ultradian rhythm and that its signaling manipulation alters ultradian periodicity (44). This suggests that dopamine is involved in mediating ultradian rhythms. Furthermore, the ultradian feeding rhythm in the common vole is known to synchronize between individuals, suggesting that some of the ultradian rhythms have functional significance (39).

To investigate the circadian and ultradian rhythms and their couplings, the running wheel activity of wild-type mice, heterozygous PER2::LUC knockin mice, and *Per1/2/3* KO mice was measured in several conditions. First, the behavior of a control group containing seven heterozygous PER2::LUC knockin Mice and a wild-type littermate in constant darkness was established. Then, the behavior of *Per1/2/3* KO mice in constant darkness with and without methamphetamine was evaluated. Lastly, the behavior of *Per1/2/3* KO mice was measured with and without methamphetamine in constant darkness and in constant light, as well as in conditions of 12 h darkness and 12 h light alternating for several days.

Data were analyzed using novel methods for tracing instantaneous frequencies (30) and mutual couplings (32, 45) in time, based on the theory for discerning time-resolved oscillatory dynamics (35, 36, 46). Characteristic frequencies of relevant oscillations on time-scales between days and minutes were calculated over time using the wavelet transform and ridge extraction (28, 30). The frequency content was additionally checked using harmonic analysis (47) to establish the presence of modes and distinguish them from high harmonic components. Once modes were established, wavelet bispectral analysis (32) and dynamic Bayesian inference (DBI) (27, 31) were used to infer directions of coupling between modes under various experimental conditions, as outlined above.

Our results demonstrate that the circadian rhythm is highly stable in wild-type and PER2::LUC knockin mice. Knocking out *Per1/2/3* genes reduces the power of the circadian rhythm and introduces irregularity. Methampetamine reinstates an irregular, nonstationary, circadian rhythm in the absence of canonical clock genes. When evaluated using a time-localized approach, there exists clear evidence of birhythmicity (48–50) in *Per1/2/3* KO mice following methamphetamine administration. Additionally, for the first time, we demonstrate changes in the coupling between modes following methamphetamine exposure. The dynamic, time-varying, characteristics of the MASCO may have implications regarding sleep disorders following stimulant exposure (51–54), particularly in individuals with attention deficit/hyperactivity disorder (ADHD) (55–57), and in several other conditions including schizophrenia, Alzheimer's disease, and autism spectrum disorder (58–63). A clearer understanding of the mechanisms behind the irregular nature of the MASCO may elucidate dynamic aspects of circadian regulation.

Results

Highly regular circadian oscillations in wild-type and PER2::LUC knockin mice

To determine the behavior of the canonical circadian rhythm, wheel running activity of a control group containing heterogeneous PER2::LUCIFERASE knockin mice, and one wild-type littermate, was assessed in constant darkness ($n = 8$). The wavelet transform in Fig. 1B demonstrates highly regular nature of the circadian rhythm in this control group. Furthermore, the time-averaged power in Fig. 1C demonstrates a sharp peak centered ~24 h. The average frequency of this oscillation in the control group was 23.9 ± 0.1 h. Two cohorts of wild-type mice ($n = 5$, $n = 6$) were also measured in constant darkness, over a shorter recording interval (20 and 21 days, respectively). The circadian oscillation was confirmed as being highly regular in these mice. Their group median circadian frequencies were 23.4 ± 0.2 h and 23.6 ± 0.2 h, respectively. Full details, including the frequency of each mode for each mouse and their time-localized powers, are given in the Supplementary material. The presence of ultradian and high-frequency modes were also detected in the heterozygous PER2::LUC knockin and wild-type mice, but at a much lower power relative to the circadian rhythm.

Ultradian oscillations are prevalent in *Per1/2/3* knockout mice

Wheel running activity in a cohort of *Per1/2/3* knockout mice in constant darkness ($n = 6$, *Per1/2/3* KO DD hereafter) demonstrated significant changes to the circadian oscillation observed in wild-type and heterozygous PER2::LUC knockin mice. Instead of a single, nontime-varying mode, an intermittent quasi-circadian rhythm appeared around every 22 days, as previously reported (41). The average frequency of the most prominent oscillatory mode in the *Per1/2/3* KO DD group was 7.2 ± 0.9 h, with both the large standard deviation (SD), and Fig. 1E highlighting the time variability of this mode.

Methamphetamine exposure induces a time-varying circadian rhythm

Analysis of wheel running activity in a cohort of *Per1/2/3* knockout mice in constant darkness with methamphetamine exposure

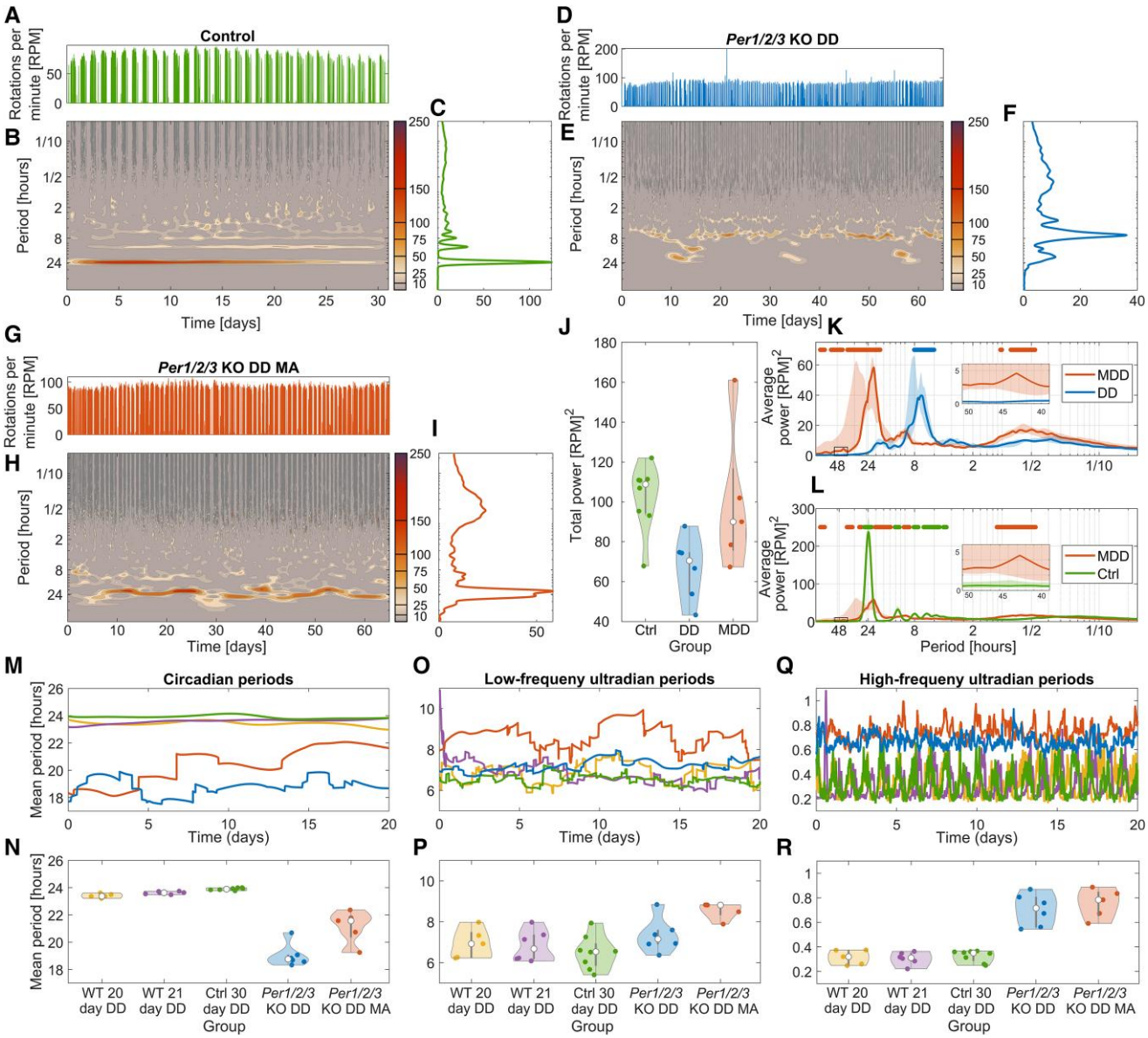

Fig. 1. Multiscale oscillatory activity in heterozygous PER2::LUC knockin, wild-type and *Per1/2/3* KO mice with and without methamphetamine administration. For all plots, yellow is used for data related to wild-type mice from the group measured for 20 days, purple is used for the wild-type group measured for 21 days, green is used for the control group measured for 30 days, blue is used for the *Per1/2/3* KO mice measured for 65 days, and red is used for the *Per1/2/3* KO mice exposed to methamphetamine for 65 days. All mice were in constant darkness. A, D, G) Time-series of wheel rotations per minute in the control group, *Per1/2/3* KO (*Per1/2/3* KO DD) mice, and *Per1/2/3* KO with methamphetamine (*Per1/2/3* KO DD MA) mice. B, E, H) Time-frequency representations of the control group, *Per1/2/3* KO DD and *Per1/2/3* KO DD MA data. C, F, I) Time-averaged power for each group, respectively. J) Total power evaluated between periods of 84 h and 4 min in each condition. The total power between the control group (Ctrl) and *Per1/2/3* KO mice is statistically significant ($P = 0.0047$ Wilcoxon rank sum, effect size =2.2, Cohens D. K, L) Group median time-averaged power plot (K) compares the *Per1/2/3* KO mice with and without methamphetamine, while (L) compares the methamphetamine *Per1/2/3* KO mice and the control group. The shading represents the 25th and 75th percentile while the circles indicate frequencies where there were significant differences between groups, with the color of the circle indicating the group with the greater power (Wilcoxon rank-sum test $P < 0.01$). M, O, Q) Group median instantaneous frequencies for the circadian and ultradian modes evaluated over time. N, P, R) Time average instantaneous frequencies for the circadian and ultradian modes for each mouse. The instantaneous frequency of each mode was obtained using ridge extraction (30).

($N = 5$, *Per1/2/3* KO DD MA) reveals the restoration of the circadian rhythm compared to the *Per1/2/3* KO DD mice. The wavelet transform in Fig. 1H, and the width of the time averaged power peak in Fig. 1I illustrate circadian behavior with significant time-variability compared to the wild-type and heterozygous PER2::LUC knockin mice. The average frequency of the circadian activity was 21.6 ± 2.5 h. Closer inspection of the time-localized power in Fig. 1H reveals that the MASCO seems to exhibit birhythmicity, seemingly switching between periods greater than and less than 24 h over time.

To further evaluate the differences following methamphetamine exposure, group median power values were compared. Figure 1K illustrates theses differences, with the colored circles representing the group with a significantly higher power at a given frequency (Wilcoxon rank sum test, $p < 0.01$) while the shaded area represents the 25/75th percentile. Circadian and high-frequency ultradian power are elevated following methamphetamine administration. Additionally, methamphetamine administration introduced a significant circabidian rhythm with period of around 2 days. A low-frequency ultradian mode was also

present in the *Per1/2/3* KO DD MA mice, albeit at a slightly elongated average period of 8.8 ± 1.3 h and reduced power compared to the *Per1/2/3* KO DD group, as Fig. 1K demonstrates.

Methamphetamine exposure induces a time-varying circadian rhythm

The frequencies of the circadian and ultradian modes were analyzed in two wild-type groups ($n = 5$ WT, 20-day DD; $n = 6$ WT, 21-day DD) to ensure that the luciferase knock-in (30-day control group) did not affect the stability of rhythms. Figure 1 demonstrates the group average (M, O, Q) and time average (N, P, R) frequencies for each mode. All wild-type mice exhibited consistent average frequency values across groups. In contrast, *Per1/2/3* KO mice displayed slightly faster circadian activity and slightly slower high-frequency ultradian activity. The frequencies of each individual mouse for the three modes are provided in the Supplementary material.

The behavioral dynamics of *Per1/2/3* KO mice in multiple conditions

The wheel ruining activity of *Per1/2/3* KO mice ($N = 8$) was assessed across a series of conditions. The behavioral rhythms generally exhibited time-varying frequencies, with the dominant oscillation changing dependent upon the experimental condition, illustrated in Fig. 2B. Initially, the mice were exposed to light/dark cycles (LD, 12 h light and 12 h dark), and they exhibited a stable daily rhythm with a period of 24 h. Subsequently, the light periods were removed, leaving the mice in constant darkness (DD). In the absence of light and with *Period* genes knocked out, the dominant oscillatory mode was at around 7 h. Following administration of methamphetamine during constant darkness (MDD), the dominant rhythm is within the circadian range. When exposed to methamphetamine in constant light (MLL), a similar behavior was observed, but at a slightly higher frequency. After methamphetamine was removed, the mice remained in constant light (LL), where the dominant period was around 4 h. When constant darkness was restored (FDD), both a 7 h and circadian mode were present. The additional circadian mode, reminiscent of the MDD condition, may suggest an enduring effect from methamphetamine in the system. The results of *Per1/2/3* KO mice both with and without methamphetamine were consistent with our previous findings. The wavelet transforms for each mouse under investigation are provided in the Supplementary material.

Methamphetamine increases total power

Comparing control group, *Per1/2/3* KO DD and *Per1/2/3* KO DD MA mice revealed that the total power was significantly different (Wilcoxon rank-sum, $P = 0.0047$, effect size = 2.2, Cohen's D)

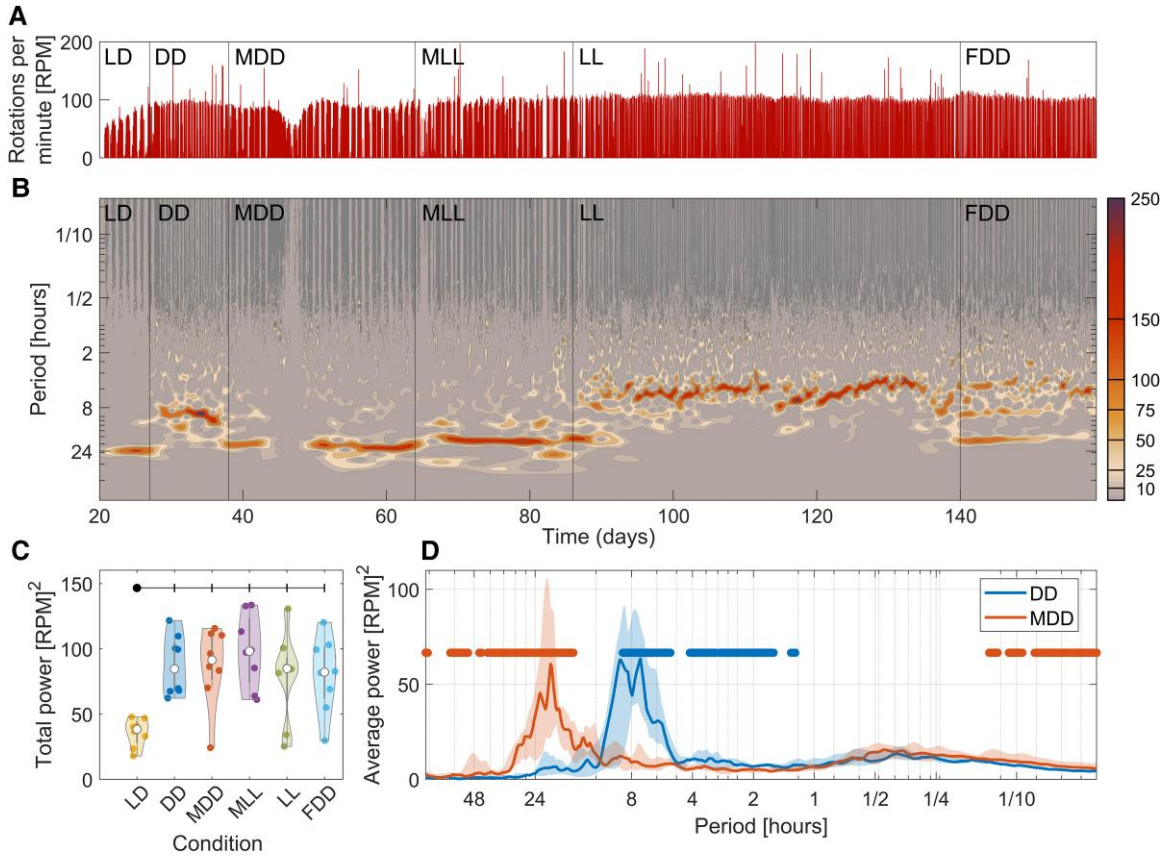

Fig. 2. The effect of different environmental and pharmacological modalities on the locomotor rhythms of *Per1/2/3* KO mice. A) time-series recorded for 139 days under varying conditions. The separate experimental conditions are denoted as follows: LD, light/dark cycles of period 24 h; DD, constant darkness; MDD, constant darkness with methamphetamine administration; MLL, constant light with methamphetamine administration; LL, constant light; FDD, final condition of constant darkness. B) Time-frequency representation across all conditions. C) The total power evaluated in a central 7 day window of each measurement modality across scales with periods between 84 h and 4 min. Circles and dashes on top of the plot denote significant differences between conditions ($P < 0.05$). D) Time-averaged power in the DD (blue) and MDD (orange) modalities. shading denotes the 25th to 75th percentiles, the bold line represents the median value across frequency and blue/orange dots represent a significant difference between groups at a given frequency ($P < 0.05$) evaluated using the Wilcoxon rank sum test.

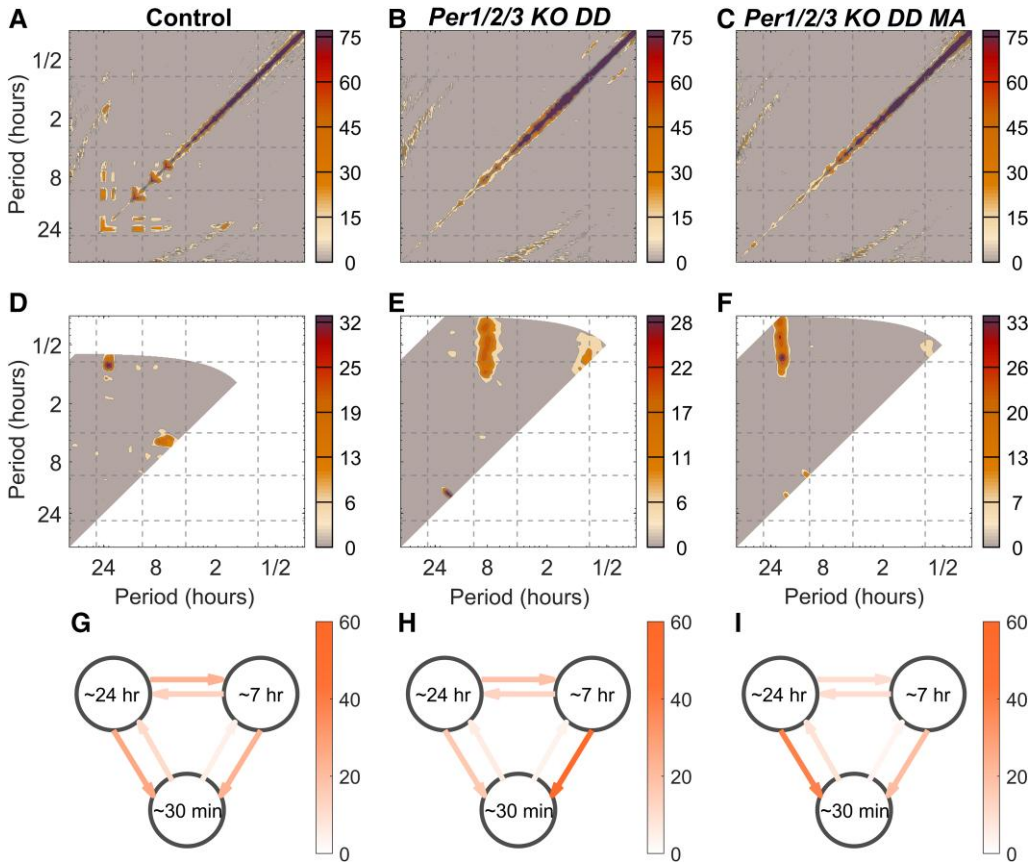

Fig. 3. Harmonic and coupling analysis between the control group (first column), *Per1/2/3* KO DD mice (second column), and *Per1/2/3* KO DD MA mice (third column). Harmonic analysis (A–C) demonstrates pronounced harmonics in the control group, arising from circadian oscillations. The colorful peaks indicate the detection of these harmonics. The diagonal line, representing the comparison of the same oscillation to itself, shows high mutual information, while off-diagonal peaks signify the presence of harmonics, such as those observed between 24 and 12 h in (A). Bispectral analysis (D–F) highlights couplings between oscillatory modes at different frequencies. Similar to harmonics, contoured peaks indicate regions of significant coupling between these modes. DBI (G–I) shows the percentage of time during which the oscillatory modes (circadian ≈24 h, low-frequency ultradian ≈7 h, high-frequency ultradian ≈30 min remained coupled throughout the time series. Increased color intensity corresponds to a longer duration of coupling between specific modes.

between the control group and *Per1/2/3* KO DD group, but not *Per1/2/3* KO DD MA and *Per1/2/3* KO DD mice. This was despite a tendency for increased total power in *Per1/2/3* KO DD MA mice. This is likely due to the reduced statistical strength owing to small sample sizes ($N_{Ctrl} = 8$, $N_{DD} = 6$, $N_{MDD} = 5$).

Total power results were also calculated in the *Per1/2/3* KO mice across the different experimental conditions. Only the LD condition total power differed significantly from the other conditions (Wilcoxon rank-sum, $P < 0.05$, Fig. 2C).

Harmonic detection

Before considering the presence of mutual coupling between modes, the independence of activity in the time-frequency domain must be ascertained. Harmonic analysis in Fig. 3A–C demonstrates the control group, *Per1/2/3* KO DD and *Per1/2/3* KO DD MA data, respectively. The control group mouse has significant evidence for harmonics of the circadian oscillation, indicating that the peaks at around 12, 8, and 4 h in the power plots of Fig. 1B and C are not independent modes. There was no evidence for harmonics in the *Per1/2/3* KO mice exposed to methamphetamine. Notably, the circabidian oscillations present in *Per1/2/3* KO DD MA mice are independent modes, and not the result of harmonics. In contrast, *Per1/2/3* KO DD mice demonstrated evidence of a harmonic in about half of the mice between 7 and 3.5 h. Harmonic analysis for each of the mice is presented in the Supplementary material.

Couplings change following methamphetamine administration

The presence of mutual coupling between modes was evaluated using bispectral analysis. Figure 3D–F indicate phase couplings between behavioral modes for the control group, *Per1/2/3* KO DD mice and *Per1/2/3* KO DD MA mice, respectively. The control group mice were measured for 30 days, hence insufficient data were present to consider the couplings to the high-frequency activity. Although a number of bands demonstrated traces of significant couplings in the control mice, these patterns were not consistent across the group (Fig. 3G and Supplementary material). Both *Per1/2/3* KO DD, Fig. 3E, and *Per1/2/3* KO DD MA, Fig. 3F, reveal the presence of couplings within the high-frequency ultradian band. In the *Per1/2/3* KO DD mice, the predominant coupling was between the ~7 h oscillation and higher frequencies. Following methamphetamine exposure the coupling between the circadian rhythm and high-frequency ultradian activity became dominant.

DBI was employed to further confirm the presence of these couplings and detect the direction of the information flow between modes. This metric was evaluated as the percentage time over which certain directional couplings were present (Fig. 3G–I). In

Per1/2/3 KO DD mice, the 7 h mode drove high-frequency activity, while in *Per1/2/3* KO DD MA mice circadian rhythms became the dominant driver (Fig. 3I).

Discussion

Circadian rhythms are a fundamental characteristic of mammalian life. To function optimally, humans are constrained to operate within a 24 h cycle. Neglecting our implicit chronobiology may lead to mental illness and disease (55–59, 61–64). While many recent discoveries have shed light upon the canonical circadian clock, less is known about alternative pacemakers which may impact these processes (15, 65). A more comprehensive understanding of these noncanonical oscillators, such as the MASCO may elucidate the mechanisms behind, for example, human sleep disorders (10) and addiction to psychostimulants (15).

Time-localized, multiscale analysis approach

Here, we apply time-localized multiscale analysis approaches to investigate behavioral dynamics following methamphetamine administration in *Per1/2/3* KO mice (33, 46, 66). The approach exploits wavelet analysis to evolve the power and frequency of the rhythms over time and allow for studying their nonstationary time-variable nature. Wavelets are usually considered as a linear method (67). Because of the time evolution they provide, they allow for studying the signatures of nonlinearities such as the occurrence of high harmonics (47), and their time-variable frequencies (68). The time-variable frequencies can then be extracted using ridge extraction (30) and in this way, frequency and phase relationships can be evaluated under different conditions. In particular, couplings between instantaneous frequencies and phases can be studied (32, 45). Couplings have been demonstrated to provide a wealth of information about the state of a system in various applications (31, 69). Here, we demonstrate how couplings change with *Per1/2/3* genes knocked out and in the presence of methamphetamine. In this way, we add an additional approach to studying periodic behavior on multiple scales to the existing methods (67, 70, 71).

Behavioral rhythms in PER2::LUC knockin and wild-type mice

To understand the effect of methamphetamine on circadian oscillations, a series of experiments were conducted. Initially, the behavioral rhythms of a control group containing heterozygous PER2::LUC knockin mice and a wild-type littermate in constant darkness were established. A circadian rhythm with a strong and distinct peak was present at 23.9 ± 0.1 h. Similarly stable circadian oscillations were found in two additional cohorts of wild-type mice, with periods of 23.4 ± 0.2 h and 23.6 ± 0.2 h respectively. The strength of this peak arises for two reasons: first, it is dominant compared to the low (5.4–8.0 h) and high (0.22–0.37 h) frequency ultradian activity, but more importantly, the frequency is highly regular and almost constant over time (Fig. 1B).

The effect of *Per1/2/3* KO on behavioral rhythms

Wheel running activity in *Per1/2/3* KO mice in constant darkness was analyzed to elucidate what happens to behavioral rhythms when genes responsible for the canonical circadian rhythm are removed. The results revealed that knocking out the *Period* genes significantly altered the circadian rhythm. *Per1/2/3* KO DD mice exhibited an intermittent quasicircadian oscillation which seemed to appear around every 22 days, supporting previous results from this type of murine sample (41). Due to the intermittent and relatively weak nature of the circadian activity, the low-frequency ultradian oscillation, which occurred at a frequency of 7.2 ± 0.9 h, was dominant, as demonstrated in Fig. 1E.

The impact of methamphetamine exposure upon circadian and ultradian dynamics

The effect of methamphetamine upon *Per1/2/3* KO mice in constant darkness was established. A peak in power around the circadian frequencies was detected. However, while methamphetamine is able to reinstate a circadian oscillation, we found several characteristic features of the data are altered. The average period of circadian activity in the *Per1/2/3* KO DD MA group occurred at 21.6 ± 2.5 h, compared to 23.9 ± 0.1 h in the control group. The reduced SD in the control group indicates a lack of time variability. In contrast, the peak MASCO frequency in the *Per1/2/3* KO DD MA mice varied significantly over time (Fig. 1H) and was much less regular. Closer inspection revealed birythmicity between modes at periods slightly longer and shorter than 24 h, in agreement with previous findings (9, 49, 72). The ultradian mode present in the *Per1/2/3* KO DD mice persisted following methamphetamine administration, though with reduced intensity, and an elongated period of 8.8 ± 1.3 h. Total power indicated that methamphetamine administration restored activity levels similar to those observed in the control group. Methamphetamine administration also significantly elevated high-frequency ultradian activity compared to both the control group and *Per1/2/3* KO DD mice, suggesting erratic, quick bouts of activity, likely associated with methamphetamine-induced hyperactivity in mice (73–75). Moreover, methamphetamine exposure induced a circabidian oscillation, a documented behavior in rodents (23, 76).

Couplings between circadian and ultradian rhythms

Elongated recordings for the *Per1/2/3* KO DD mice enabled harmonic and coupling analyses between modes. Harmonic analysis confirmed that the circadian, low-frequency ultradian and high-frequency ultradian modes observed were independent. Importantly, the circabidian oscillation induced by methamphetamine was also confirmed as an independent mode. Bispectral analysis revealed that a significant coupling existed between the low- and high-frequency ultradian activity in the *Per1/2/3* KO mice without methamphetamine, supporting previous findings (41). When *Per1/2/3* KO mice were exposed to methamphetamine, the significant coupling was instead detected between the circadian and high-frequency activity. DBI was subsequently employed to confirm the results of the bispectral analysis and determine the direction of information flow between the behavioral modes. DBI confirmed the presence of couplings. The direction of information flow was from the slower to the quicker oscillation in each case. These results highlight that not only the presence of modes but also the interactions between them are altered following methamphetamine administration.

Influence of methamphetamine and light on *Per1/2/3* KO mice.

Finally, *Per1/2/3* KO mice were exposed to a series of different light and pharmacological conditions. Following methamphetamine exposure in both constant darkness and constant light, an ~24 h periodicity was restored, supporting the findings in *Per1/2/3* KO DD MA mice reported above. The results also demonstrated that

methamphetamine may have long-term effects upon the system as the constant darkness condition following drug exposure still contained significant evidence of sustained 24 and 7 h oscillations (Fig. 2B). It has been previously reported that LL exposure rescued the circadian behavioral rhythm in *Cry1/2* double knockout mice (77, 78). Therefore it is possible that the behavioral circadian rhythm we observed in DD is due to LL exposure. While these oscillations are known to be present (65, 79), further clarification of their duration and intensity may have important implications for future experimental designs.

Phenomenological model

A simple phenomenological model was utilized to further validate the observed behaviors against a ground truth. Simulating the time series as several interacting phase oscillators yielded power results strikingly similar to those from the analyzed experimental data. Furthermore, altering the coupling strength between oscillators yields the same outputs as the experimentally derived coupling results, as demonstrated in Fig. 4 and the Supplementary material. The similarity between experimental and phenomenological model derived results validates the nonautonomous phase network dynamics framework used in the analysis (33, 46), while also verifying our interpretation of the results using a ground truth.

MASCO and internal dissociation

Previous studies on humans isolated from social and natural environments have demonstrated a phenomenon called internal dissociation, where the sleep-wake cycle shifts to either a longer (30-h) or shorter (20-h) rhythm, despite the body's core temperature maintaining an ~24-h cycle (80). Although our study was conducted in mice, the behavioral rhythms observed following methamphetamine administration closely resemble those during internal dissociation in the human sleep-wake cycle. This similarity suggests that the MASCO may play a crucial role in regulating the human sleep-wake cycle (81). The involvement of the MASCO may partially explain the sleep disorders frequently reported in individuals treated with stimulants, such as those with ADHD (55–57).

Conclusion and future work

Our results suggest that two main factors are crucial for period determination in wheel running activity: the use of time-localized analysis approaches, which do not average over transient dynamics, and the use of extended recording intervals, sufficient to capture the inherent time-variability of the MASCO. The instability of the MASCO may suggest that *Period* genes play a crucial role in regulating the time-variability of the circadian rhythm, or alternately that the MASCO itself is inherently time-variable. Additionally, the multiscale nature of the investigation enabled circadian, circabidian and ultradian oscillations to be considered simultaneously, whilst also being a sufficient length for coupling analysis.

The presence of an additional low-frequency (~3.5 h) ultradian rhythm has been previously reported in *Per1/2/3* KO DD mice (41). However, in the present study, there was insufficient evidence to classify this period as a distinct mode. Future investigations involving mice under varied experimental conditions and extended measurement intervals are necessary to confirm or contradict its existence.

Future investigations may utilize this approach to evaluate dynamical characteristics in different experimental conditions and animal populations. For instance, analysis of alternative noncanonical oscillators, such as the food-entrainable oscillator, and comparison to the MASCO may provide evidence regarding a proposed common dopaminergic basis (82). Additionally, investigating the number of cycles which behavioral patterns persist for in the absence of the stimuli that induced them may inform future experimental design.

Time-resolved analysis methods offer a wealth of additional information and insight into the mechanisms of complex behavior, unlike detrended fluctuation analysis which provides information about the balance between randomness and regularity (70, 71). By considering behaviors throughout time, one can observe temporal variability that may betray underlying biological implications (83). Circadian rhythms are intimately linked to several pathologies, both mental and physical (84–86). By applying novel time-series analysis approaches one may reveal an abundance of information, previously disregarded as stochastic, and move towards a more complete description of circadian regulation.

Materials and methods

Animals

All mouse experiments were approved by the Institutional Animal Care and Use Committee at UT Southwestern Medical Center (Protocol #2013-0035 and #2016-10376-G).

Bmal1 KO mice are commonly used for studying the functional significance of the circadian rhythm because this single gene knockout can disrupt molecular circadian oscillations entirely. However, *Bmal1* KO mice have a significantly reduced life span and experience premature ageing (87). Therefore, they are inappropriate for studies which require long-term behavioral recordings. Although *Per1/2/3* KO mice have disrupted molecular circadian rhythms, no notable health issues have been reported (48), hence their use in this study.

In the initial investigation, $N = 8$ *Per1/2/3* KO mice (Yamazaki Lab Experiment #74; 4 males, 4 females; 5–8 months old; C57BL/6J or C57BL/6J and C57BL/6N mixed backgrounds (41, 50)) were measured in a variety of conditions. Mice were first exposed to 12 h light, 12 h dark cycles for 7 days (LD, light intensity ~450 lux at cage level) and then kept in constant darkness for 11 days (DD). Subsequently, methamphetamine was administered through drinking water for 26 days while they remained in constant darkness (MDD). The mice were then exposed to constant light for 22 days while methamphetamine administration continued (MLL, light intensity ~170 lux at cage level). Subsequently, methamphetamine was removed while still in constant light for 54 days (LL, light intensity ~170 lux at cage level). The final 24 days of the experiment were conducted in constant darkness for 24 days (FDD). This group is referred to as "*Per1/2/3* KO DD multiple conditions" throughout the text.

To better understand the multiscale behavioral changes following exposure to methamphetamine across elongated measurement intervals, five additional cohorts of mice were investigated. A cohort of heterozygous PER2:luciferase knockin mice ($n = 7$) and one wild-type littermate ($n = 1$), were used as a comparison point (Yamazaki Lab Experiment #17; 5 males, 3 females; 1.3–9.5 months old; C57BL/6J background (88, 89)). These mice were kept in constant darkness for 95 days without methamphetamine. General cage activity was recorded with an infrared motion detector in the cage without a running wheel for the first 10 days, then in a cage containing a locked running wheel for 11 days. After that, the running wheel was unlocked and both general activity and wheel running activity were recorded for 20

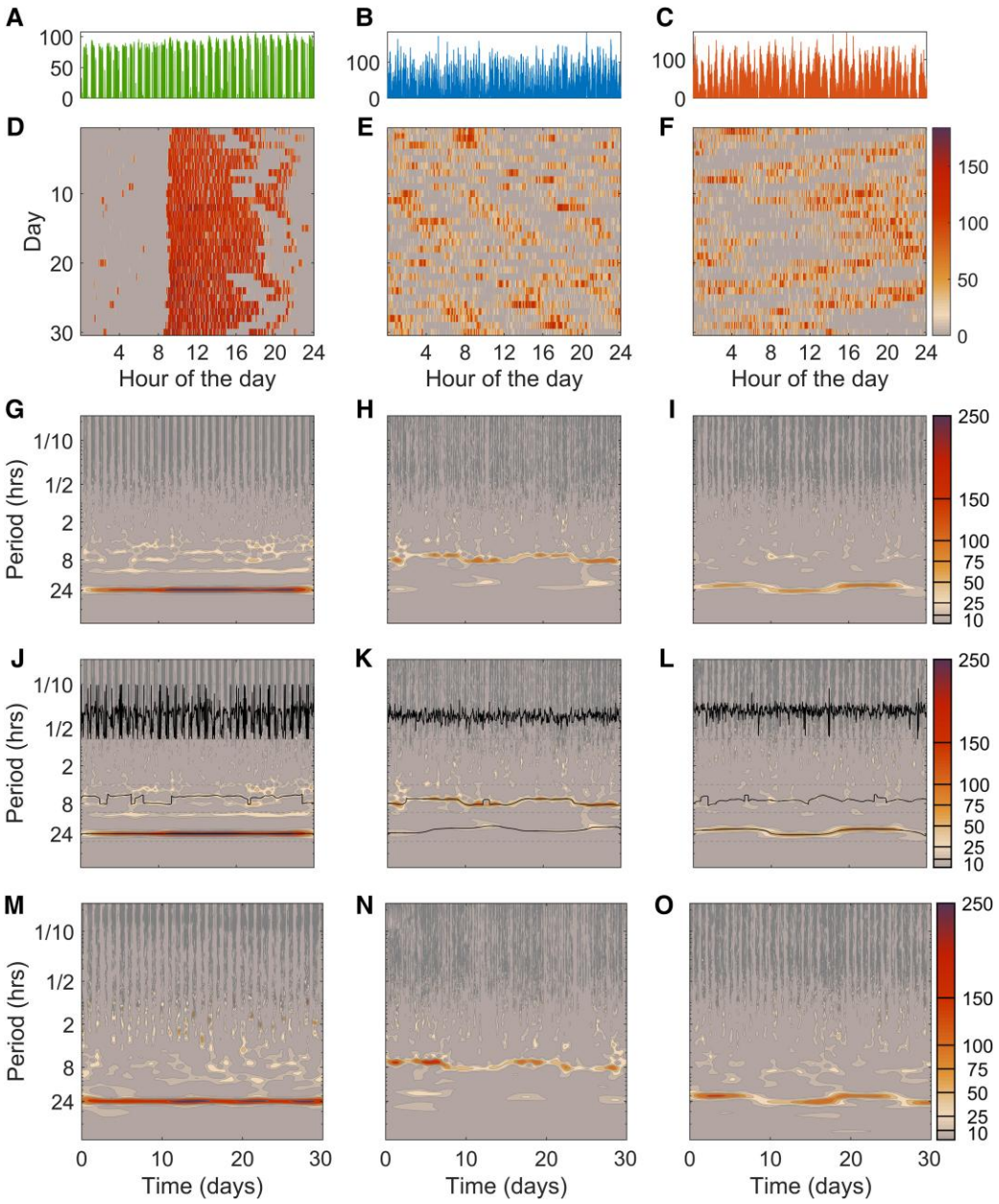

Fig. 4. Comparison between the time and time-frequency domains for evaluating characteristic features of underlying dynamics. Each mouse condition is represented by a column; the control group (first column), *Per1/2/3* KO DD mice (second column), and *Per1/2/3* KO DD mice with methamphetamine (third column). A–C) Thirty days of the recorded wheel running activity per minute. D–F) Actograms representing the amount of wheel turns for each minute of activity. G–I) Time-frequency representation of each condition. J–L) Extracted ridges for each of the time-frequency representations. In each frequency band, the ridges follow a high amplitude peak through time. The phases at each of these points are used in the coupling analysis. M–O) Data generated by the phenomenological model which was used to validate conclusions.

days. The wheel was then locked once again for a further 21 days, before being unlocked for the final 30 days. Here, we analyzed the last 30 days of running wheel activity. This group is referred to as "the control group" throughout the text.

Heterozygous *PER2*:luciferase knockin mice were used as the control group due to their elongated recordings in constant darkness, which enabled coupling analysis. To confirm that the power results observed in these knockin mice are consistent with those in pure wild-type cohorts, two groups of wild-type mice recorded over shorter intervals were analyzed.

In one of these experiments, $n = 5$ wild-type male mice (Yamazaki Lab experiment #17B; 5 weeks old at the beginning of the experiment; strain C57BL/6N), were included. Mice were first exposed to 12 h light, 12 h dark cycles for 7 days. Subsequently, they were kept in constant darkness for the duration of the recordings analyzed in the present study. On the 22nd day, the mice were moved into cages containing a locked wheel, while remaining under DD. On day 33, the running wheels were unlocked and the running wheel activity could be measured for the subsequent 20 days, until they were once again locked. This procedure resulted in a 20 day recording of running wheel activity in wild-type mice in DD. The time-localized powers of these mice are summarized in the Supplementary material. This group is referred to as "wild-type 20 days."

Additionally, $n = 6$ males (Yamazaki lab experiment #20;) were analyzed; all mice were between 7 and 8 weeks old at the

beginning of the experiment; strain: C57BL/6J. The mice were exposed to light/dark 12 h repeats for 7 days. A constant darkness protocol was then initiated. After 21 days, the mice were switched to a cage with a wheel to measure movement. They remained in this cage for another 21 days in constant darkness, and the wheel allowed their movement to be tracked during this interval. The time-localized power for each of the six mice measured under these conditions is shown in the Supplementary material. This group is referred to as "wild-type 21 days."

A cohort of *Per1/2/3* KO mice (Yamazaki Lab Experiment #86; three males, four females; 3.5–8.5 months old; C57BL/6J background with cfos-shGFP transgene (90)) were initially exposed to constant light (~220 lux at cage level) for 26 days then kept in constant darkness for 65 days without methamphetamine exposure. A male mouse (#2 in the Supplementary material) was excluded as the entire recording length was not completed. The 65 days of running wheel activity in constant darkness were analyzed in this manuscript. This group is referred to as "*Per1/2/3* KO DD."

Another cohort of *Per1/2/3* KO mice (Yamazaki Lab Experiment #54; one male, four females; 4.5–5.5 months old; C57BL/6J or C57BL/6J and C57BL/6N mixed background) were kept in DD for 27 days without methamphetamine, before being exposed to methamphetamine for the subsequent 101 days. The first 65 days of activity during methamphetamine administration was analyzed and is referred to as "*Per1/2/3* KO DD MA."

Each mouse was housed individually in a plastic cage (length × width × height: 29.5 × 11.5 × 12.0 cm) containing running wheels of diameter 11 cm. Wheel revolutions were continuously recorded every minute by the ClockLab system (Actimetrics, Wilmette, IL, USA). As described above, general cage activity was monitored with a passive infrared sensor (product ID 189, Adafruit, New York City, NY, USA) placed above the cages without a running wheel or with locked running wheels, however those data were not analyzed in the current study. The cages were placed in light-tight ventilated cabinets and the temperature, humidity, and light intensity inside the cabinet were recorded every 5 min by Chamber Controller software (Actimetrics, Wilmette, IL, USA). The white LEDs inside the cabinet were controlled by the Chamber Controller software. Cages and water bottles were changed once every 3 weeks. An infrared viewer (FIND-R-SCOPE Infrared Viewer; FJW Optical Systems, Inc., Palatine, IL, USA) was used to perform maintenance in the dark without exposing mice to visible light. For methamphetamine administration, water bottles were replaced with drinking (tap) water containing 0.005% methamphetamine (Sigma-Aldrich, St. Louis, MO, USA). Water bottles containing methamphetamine were changed once every 3 weeks. During the experiment mice had *ad liberum* access to food and regular or methamphetamine water.

Time-series length

Elongated time-series are required to reduce the measurement uncertainty for the following reasons. Firstly, time-varying modes require many cycles to accurately determine the frequency. In addition, it enabled the avoidance of transitory periods when switching between measurement conditions. Thirdly, couplings between modes require a minimum number of cycles to be detected. Asymptotic approaches treat data as stationary by measuring only a minimal number of cycles and averaging across time. In contrast, the approaches presented here harness the maximal amount of information by explicit consideration of time-localized behavior.

Time-resolved analysis

Evaluating multiscale oscillatory behavior requires methods that can effectively extract information across wide-ranging scales and time periods (68). Without explicitly considering the time-localized, multiscale dynamics, time-series that contain multiple deterministic modes might be incorrectly interpreted as noise (33). The wavelet transform enables such a representation of the data,

$$W_T(s, t) = \int_{-L/2}^{L/2} \Psi(s, u - t) f(u) du, \quad (1)$$

where the mother wavelet, $\Psi(s, t)$, is expanded and contracted to optimize the trade off between time-localization and frequency resolution at a given scale, akin to changing the focus on a camera to increase image sharpness. In contrast, Fourier-based approaches use a single window to obtain information across all frequencies, leading to sub-optimal resolution. Here, the lognormal wavelet was used due its superior logarithmic frequency resolution (28). In the frequency domain, it is defined as

$$\hat{\psi}(\omega) = e^{-(\omega_0 \log \omega)^2/2}, \quad \text{where } \omega > 0, \quad (2)$$

where $\omega_0 = 2\pi f_0$ is the frequency resolution parameter of the wavelet. As $\log \omega$ is the argument of this wavelet, it is particularly well suited to the logarithmic frequency resolution of the transform.

The wavelet transform facilitates multiscale evaluation of time-series (29). This enables the simultaneous evaluation of oscillatory activity taking place over days, hours, minutes, and seconds. In contrast, actograms demonstrate information regarding only the most prominent oscillation. As demonstrated in Fig. 4, this is helpful for illustrating the highly regular, circadian behavior of the wild-type or heterozygous PER2::LUC knockin mice; however, this approach is inappropriate when multiple time-varying modes are present simultaneously. As such, the time-frequency representation unlocks a wealth of information compared to purely time domain methods. It also allows for time-localized features in the behavior to be identified and evaluated.

Total power

Total power can be thought of as the total energy ($\mathcal{E}$) content in the signal (91). In the present investigation, this is defined as

$$\mathcal{E} = \frac{1}{T} \int_0^T \int_{1/2\pi f_{min}}^{1/2\pi f_{max}} \frac{1}{s} |W_T(s, t)|^2 ds dt, \quad (3)$$

where T is the total time, and $f_{\min}, f_{\max}$ represent the minimum and maximum frequencies used when calculating the wavelet transform. The logarithmic frequency distribution resulting from the wavelet transform was explicitly considered when performing the integral. When analyzing multiple conditions in the same experiment, total power was evaluated across the central 7 days to reduce edge effects.

Harmonic analysis

Spectral peaks are obtained from a mathematical description of time series and are not necessarily linked to physical oscillatory systems or modes. In the case of nonlinearities, i.e. when the signal is not of sinusoidal shape, many high harmonic components can occur belonging to the activity of a single mode. When the rhythms are strictly periodic the detection of high harmonics is relatively straightforward because they appear at commensurate frequencies of the basic frequency. However, when the rhythms have variable, or nonstationary frequencies, the detection of

high harmonics is a demanding task. To determine whether the detected frequency peaks correspond to independent modes, or the peaks are in harmonic relationship, we conduct harmonic analysis (47). This method evaluates mutual information between time-localized phases across frequency bands. If sufficient shared phase information between a fundamental frequency and its harmonics exceeds a surrogate threshold, then the relationship can be considered as harmonic. For details of the method for surrogate data analysis, see below and Ref. (92).

Ridge extraction

The underlying oscillatory modes may be harnessed to evaluate their changing power and phase over time (30). The first step here is to find the ridge curve; a region in the time-frequency domain with a series of amplitude/power peaks and their corresponding phases. Tracing these modes in the time-frequency domain can reveal time-localized amplitudes and phases.

Coupling

Once the independent modes are identified, the presence and direction of their mutual couplings and interactions can be investigated (31). The coupling analyses presented here focuses on phase relationships, independent of amplitude dynamics. The presence of couplings may be detected by bispectral analysis (32), while the direction and duration of coupling can be deduced using DBI (31).

Bispectral analysis

Wavelet bispectral analysis facilitates the detection of couplings between and/or within time-series (32). Here, we apply autobispecral analysis to ascertain the putative presence of coupling between modes within a single time series; that derived from the wheel running activity of mice. The wavelet bispectrum B_W measures the amount of phase coupling between modes at scales s_1 and s_2 as,

$$B_W(s_1, s_2) = \int_T W_T(s_1, \tau) W_T(s_2, \tau) W_T^*(s, \tau) d\tau, \quad (4)$$

during a time interval, T (93) where,

$$\frac{1}{s_1} + \frac{1}{s_2} = \frac{1}{s}. \quad (5)$$

For further details see (32). Surrogate analysis is also applied to verify results.

Dynamical Bayesian inference

To ascertain the direction of phase information flow between oscillators, we apply DBI (45). This approach infers the coupling function between oscillators by applying Bayes theorem and using both prior and current information via a windowed approach across the time series (27). From the coupling functions, we derive coupling strength over several sequential windows. The number of windows over which the coupling strength exceeds a predefined surrogate threshold defines the coupling time; a metric representing the duration over which a coupling is present.

Statistical analysis

Due to the non-Gaussian distribution of the data, Wilcoxon rank-sum test was used to compare groups. A P-value of 0.05 was used as a significance threshold when comparing groups evaluated over 6 days, while 0.01 was used as a threshold for the longer recordings as the additional amount of information enabled a reduced threshold.

Once the instantaneous frequencies over time were obtained using ridge extraction, their mean and SD were calculated. In this way, average frequencies and their SD of the individual modes for each mouse were obtained. Group averages were obtained as medians of the average instantaneous frequencies and as medians of the SD.

Surrogates

To assess whether obtained coupling results are genuine or spurious, we employ surrogate data (92). Connectivity analyses always detect a baseline level of interaction, even between independent time-series, especially when the data are short relative to the frequencies of interest. Surrogates help establish a threshold to minimize the impact of these spurious measurements. The goal when generating surrogates is to maintain the same statistical properties to measured data, with the exception of the specific characteristic being investigated (92, 94).

The same analysis performed between experimental data is applied to the generated surrogate data. This establishes a baseline of measurement outcomes in the absence of true coupling. The process is repeated many times, and a percentile of these surrogate outputs is used to set a threshold value. Results exceeding this threshold are then considered statistically significant (92).

For DBI, 19 cyclic phase permutation surrogates were generated to randomize the phase behavior, while for bispectral analysis 19 iterative amplitude adjusted Fourier transform surrogates were used. In both cases, a 95th percentile threshold was implemented.

Acknowledgments

The authors thank Crystal N. Bettilyon and Alexandra J. Brown for assistance with generating experimental mice and for animal care during behavior recording.

Supplementary Material

Supplementary material is available at *PNAS Nexus* online.

Funding

S.J.K.B. is jointly supported by the Engineering and Physical Sciences Research Council (EPSRC), UK and the MyMind GmbH – Brainhero, Vienna, Austria (grant no. EP/T518037/1). MA extends his appreciation to the Deanship of Scientific Research at Northern Border University, Arar, 73311, KSA for funding the research work through the project number "NBU-FFR-2025-0000-01". The work of S.Y. is supported by National Science Foundation grants IOS-1419477, IOS-1931115, National Institutes of Health grants R21 NS099809, R01NS114527. The work of A.S. is funded through the Sony Research Award Program and the Engineering and Physical Sciences Research Council, UK (grant no. EP/X004597/1). The development of the MODA toolbox used for analyses has been supported by the Engineering and Physical Sciences Research Council (UK) [grant nos EP/100999X1 and EP/M006298/1], the European Union projects BRACCIA (Brain, Respiration and Cardiac Causalities in Anaesthesia) [517133] and COSMOS (Complex Oscillatory Systems: Modeling and Analysis) [642563], the Action Medical Research (United Kingdom) Project [GN1963], and the Slovenian Research Agency (program no. P20232). The High End Computing facility at Lancaster University was used for some of the computations.

Author Contributions

S.J.K.B.: data curation, software, formal analysis, investigation, methodology, writing-original draft, writing-review and editing investigation; M.A.: formal analysis, investigation, methodology, software; S.Y.: conceptualization, resources, data curation, supervision, project administration, writing-review and editing; A.S.: conceptualization, supervision, funding acquisition, investigation, visualization, methodology, project administration, writing-review and editing.

Data Availability

The data analyzed in this investigation are available at https://doi.org/10.17635/lancaster/researchdata/683. The majority of the analyses were done using the MODA (Multiscale Oscillatory Dynamics Analysis) software toolbox, which is publicly available at https://github.com/luphysics/MODA (95).

References

1 Barger LK, Lockley SW, Rajaratnam SMW, Landrigan CP. 2009. Neurobehavioral, health, and safety consequences associated with shift work in safety-sensitive professions. *Curr Neurol Neurosci Rep*. 9(2):155–164.

2 Fagiani F, *et al.* 2022. Molecular regulations of circadian rhythm and implications for physiology and diseases. *Signal Transduct Target Ther*. 7(1):41.

3 Chen K, *et al.* 2024. Biological clock regulation by the PER gene family: a new perspective on tumor development. *Front Cell Dev Biol*. 12:1332506.

4 Ralph MR, Foster RG, Davis FC, Menaker M. 1990. Transplanted suprachiasmatic nucleus determines circadian period. *Science*. 247(4945):975–978.

5 Inagaki N, Honma S, Ono D, Tanahashi Y, Honma K-I. 2007. Separate oscillating cell groups in mouse suprachiasmatic nucleus couple photoperiodically to the onset and end of daily activity. *Proc Natl Acad Sci U S A*. 104(18):7664–7669.

6 Weaver DR. 1998. The suprachiasmatic nucleus: a 25-year retrospective. *J Biol Rhythms*. 13(2):100–112.

7 Pendergast JS, Yamazaki S. 2018. The mysterious food-entrainable oscillator: insights from mutant and engineered mouse models. *J Biol Rhythms*. 33(5):458–474.

8 Brown AJ, Pendergast JS, Yamazaki S. 2019. Focus: clocks and cycles: peripheral circadian oscillators. *Yale J Biol Med*. 92(2):327.

9 Honma K-I, Honma S. 2009. The SCN-independent clocks, methamphetamine and food restriction. *Eur J Neurosci*. 30(9):1707–1717.

10 Taufique SK, Ehichioya D, Pendergast J, Yamazaki S. 10 2022. Genetics and functional significance of the understudied methamphetamine sensitive circadian oscillator (MASCO). *F1000Res*. 11:1018.

11 Bell-Pedersen D, *et al.* 2005. Circadian rhythms from multiple oscillators: lessons from diverse organisms. *Nat Rev Genet*. 6(7):544–556.

12 Nakamura TJ, *et al.* 2023. Long days restore regular estrous cyclicity in mice lacking circadian rhythms. *Heliyon*. 9(6):e16970.

13 Cox KH, Takahashi JS. 2019. Circadian clock genes and the transcriptional architecture of the clock mechanism. *J Mol Endocrinol*. 63(4):R93–R102.

14 Bae K, Weaver DR. 2007. Transient, light-induced rhythmicity in mPer-deficient mice. *J Biol Rhythms*. 22(1):85–88.

15 Mohawk JA, Baer ML, Menaker M. 2009. The methamphetamine-sensitive circadian oscillator does not employ canonical clock genes. *Proc Natl Acad Sci U S A*. 106(9):3519–3524.

16 Colwell CS, *et al.* 2003. Disrupted circadian rhythms in VIP-and PHI-deficient mice. *Am J Physiol*. 285(5):R939–R949.

17 Brown TM, Hughes AT, Piggins HD. 2005. Gastrin-releasing peptide promotes suprachiasmatic nuclei cellular rhythmicity in the absence of vasoactive intestinal polypeptide-VPAC2 receptor signaling. *J Neurosci*. 25(48):11155–11164.

18 Aton SJ, Colwell CS, Harmar AJ, Waschek J, Herzog ED. 2005. Vasoactive intestinal polypeptide mediates circadian rhythmicity and synchrony in mammalian clock neurons. *Nat Neurosci*. 8(4):476–483.

19 Hughes ATL, Piggins HD. 2008. Behavioral responses of Vipr2–/– mice to light. *J Biol Rhythms*. 23(3):211–219.

20 Power A, Hughes ATL, Samuels RE, Piggins HD. 2010. Rhythm-promoting actions of exercise in mice with deficient neuropeptide signaling. *J Biol Rhythms*. 25(4):235–246.

21 Hughes ATL, *et al.* 2021. Timed daily exercise remodels circadian rhythms in mice. *Commun Biol*. 4(1):761.

22 van der Veen DR, Gerkema MP. 2024. Re-scoping ultradian rhythms in the context of metabolism. *Front Psychol*. 15:1504879.

23 Markam PS, *et al.* 2025. Mesolimbic dopamine neurons drive infradian rhythms in sleep-wake and heightened activity state. *Sci Adv*. 11(1):eado9965.

24 Barnes SJK, Stefanovska A. 2021. Physics of cellular energy metabolism. *Contemp Phys*. 62(3):125–143.

25 Goldbeter A. 2008. Biological rhythms: clocks for all times. *Curr Biol*. 18(17):R751–R753.

26 Reid KJ. 2019. Assessment of circadian rhythms. *Neurol Clin*. 37(3):505–526.

27 Stankovski T, Duggento A, McClintock PVE, Stefanovska A. 2014. A tutorial on time-evolving dynamical Bayesian inference. *Eur Phys J*. 223:2685–2703.

28 Iatsenko D, McClintock PVE, Stefanovska A. 2015. Linear and synchrosqueezed time–frequency representations revisited: overview, standards of use, resolution, reconstruction, concentration, and algorithms. *Digit Signal Process*. 42(2):1–26.

29 Iatsenko D. *Nonlinear mode decomposition: theory and applications* Springer, 2015.

30 Iatsenko D, McClintock PVE, Stefanovska A. 2016. Extraction of instantaneous frequencies from ridges in time–frequency representations of signals. *Signal Process*. 125(8):290–303.

31 Stankovski T, Pereira T, McClintock PVE, Stefanovska A. 2017. Coupling functions: universal insights into dynamical interaction mechanisms. *Rev Mod Phys*. 89(4):045001.

32 Newman J, Pidde A, Stefanovska A. 2021. Defining the wavelet bispectrum. *Appl Comput Harmon Anal*. 51(18):171–224.

33 Adams JR, Newman J, Stefanovska A. 2023. Distinguishing between deterministic oscillations and noise. *Eur Phys J*. 232(20):3435–3457.

34 Barnes SJK, Bjerkan J, Clemson PT, Newman J, Stefanovska A. 2024. Phase coherence—a time-localized approach to studying interactions. *Chaos*. 34(7):073155.

35 Newman J, Lucas M, Stefanovska A. 2021. Stabilization of cyclic processes by slowly varying forcing. *Chaos*. 31(12):123129.

36 Newman J, Scott JP, Rowland Adams J, Stefanovska A. 2024. Intermittent phase dynamics of non-autonomous oscillators through time-varying phase. *Phys D Nonlinear Phenom*. 461(4010):134108.

37 Prendergast BJ, Zucker I. 2016. Ultradian rhythms in mammalian physiology and behavior. *Curr Neurobiol*. 40:150–154.

38 Goh GH, Maloney SK, Mark PJ, Blache D. 2019. Episodic ultradian events–ultradian rhythms. *Biology (Basel)*. 8(1):15.
39 Gerkema MP, Daan S, Wilbrink M, Hop MW, van der Leest F. 1993. Phase control of ultradian feeding rhythms in the common vole (*Microtus arvalis*): the roles of light and the circadian system. *J Biol Rhythms*. 8(2):151–171.
40 Yang S, *et al*. 2022. Coupling-dependent metabolic ultradian rhythms in confluent cells. *Proc Natl Acad Sci U S A*. 119(45): e2211142119.
41 Morris M, Yamazaki S, Stefanovska A. 2022. Multiscale time-resolved analysis reveals remaining behavioral rhythms in mice without canonical circadian clocks. *J Biol Rhythms*. 37(3): 310–328.
42 van Rosmalen L, Hut RA. 2021. Negative energy balance enhances ultradian rhythmicity in spring-programmed voles. *J Biol Rhythms*. 36(4):359–368.
43 Ootsuka Y, *et al*. 2009. Brown adipose tissue thermogenesis heats brain and body as part of the brain-coordinated ultradian basic rest-activity cycle. *Neuroscience*. 164(2):849–861.
44 Blum ID, *et al*. 2014. A highly tunable dopaminergic oscillator generates ultradian rhythms of behavioral arousal. *Elife*. 3: e05105.
45 Stankovski T, Duggento A, McClintock PVE, Stefanovska A. 2012. Inference of time-evolving coupled dynamical systems in the presence of noise. *Phys Rev Lett*. 109(2):024101.
46 Lucas M, Newman J, Stefanovska A. Synchronisation and non-autonomicity. In: McClintock PVE, Stefanovska A, editors. *Physics of biological oscillators: new insights into non-equilibrium and non-autonomous systems*. Springer, 2021. p. 85–110.
47 Sheppard LW, Stefanovska A, McClintock PVE. 2011. Detecting the harmonics of oscillations with time-variable frequencies. *Phys Rev E*. 83(1):016206.
48 Pendergast JS, Oda GA, Niswender KD, Yamazaki S. 2012. Period determination in the food-entrainable and methamphetamine-sensitive circadian oscillator (s). *Proc Natl Acad Sci U S A*. 109(35):14218–14223.
49 Pendergast JS, Niswender KD, Yamazaki S. 2013. The complex relationship between the light-entrainable and methamphetamine-sensitive circadian oscillators: evidence from behavioral studies of period-mutant mice. *Eur J Neurosci*. 38(7):3044–3053.
50 Flôres DEFL, Bettilyon CN, Yamazaki S. 2016. Period-independent novel circadian oscillators revealed by timed exercise and palatable meals. *Sci Rep*. 6(1):21945.
51 Ironside S, Davidson F, Corkum P. 2010. Circadian motor activity affected by stimulant medication in children with attention-deficit/hyperactivity disorder. *J Sleep Res*. 19(4):546–551.
52 Hasler BP, Smith LJ, Cousins JC, Bootzin RR. 2012. Circadian rhythms, sleep, and substance abuse. *Sleep Med Rev*. 16(1):67–81.
53 Antle MC, *et al*. 2012. Methylphenidate modifies the motion of the circadian clock. *Neuropsychopharmacology*. 37(11):2446–2455.
54 Ramasamy T, Doke M, McLaughlin JP, Samikkannu T. 2023. Circadian disruption and psychostimulants dysregulates plasma acute-phase proteins and circulating cell-free mitochondrial DNA. *Brain Behav Immun*. 31:100659.
55 Stein MA, Weiss M, Hlavaty L. 2012. ADHD treatments, sleep, and sleep problems: complex associations. *Neurotherapeutics*. 9(3): 509–517.
56 Becker SP. 2020. ADHD and sleep: recent advances and future directions. *Curr Opin Psychol*. 34:50–56.
57 Surman CBH, Walsh DM. 2022. Understanding the impact of stimulants on sleep in ADHD: evidence from systematic assessment of sleep in adults. *CNS Drugs*. 36(3):253–260.
58 Musiek ES, Xiong DD, Holtzman DM. 2015. Sleep, circadian rhythms, and the pathogenesis of Alzheimer disease. *Exp Mol Med*. 47(3):e148–e148.
59 Snitselaar MA, Smits MG, van der Heijden KB, Spijker J. 2017. Sleep and circadian rhythmicity in adult ADHD and the effect of stimulants: a review of the current literature. *J Atten Disord*. 21(1):14–26.
60 Vallée A, Lecarpentier Y, Guillevin R, Vallée J-N. 2020. The influence of circadian rhythms and aerobic glycolysis in autism spectrum disorder. *Transl Psychiatry*. 10(1):400.
61 Walker WH, Walton JC, DeVries AC, Nelson RJ. 2020. Circadian rhythm disruption and mental health. *Transl Psychiatry*. 10(1):1–13.
62 Lorsung E, Karthikeyan R, Cao R. 2021. Biological timing and neurodevelopmental disorders: a role for circadian dysfunction in autism spectrum disorders. *Front Neurosci*. 15:642745.
63 Martinez-Cayuelas E, *et al*. 2024. Sleep problems, circadian rhythms, and their relation to behavioral difficulties in children and adolescents with autism spectrum disorder. *J Autism Dev Disord*. 54(5):1712–1726.
64 Foster RG. 2020. Sleep, circadian rhythms and health. *Interface Focus*. 10(3):20190098.
65 Tataroglu Ö, Davidson AJ, Benvenuto LJ, Menaker M. 2006. The methamphetamine-sensitive circadian oscillator (MASCO) in mice. *J Biol Rhythms*. 21(3):185–194.
66 Clemson PT, Stefanovska A. 2014. Discerning non-autonomous dynamics. *Phys Rep*. 542(4):297–368.
67 Gao C, *et al*. 2023. Approaches for assessing circadian rest-activity patterns using actigraphy in cohort and population-based studies. *Curr Sleep Med Rep*. 9(4):247–256.
68 Clemson P, Lancaster G, Stefanovska A. 2016. Reconstructing time-dependent dynamics. *Proc IEEE*. 104(2):223–241.
69 Stankovski T, Pereira T, McClintock PVE, Stefanovska A. 2019. Coupling functions: dynamical interaction mechanisms in the physical, biological and social sciences.
70 Guzmán DA, *et al*. 2017. The fractal organization of ultradian rhythms in avian behavior. *Sci Rep*. 7(1):684.
71 Minaeva O, *et al*. 2024. Fractal motor activity during wakefulness and sleep: a window into depression recency and symptom recurrence. *Psychol Med*. 54:1–9.
72 Honma S, Yasuda T, Yasui A, Van Der Horst GTJ, Honma K-I. 2008. Circadian behavioral rhythms in Cry1/Cry2 double-deficient mice induced by methamphetamine. *J Biol Rhythms*. 23(1):91–94.
73 Honma K-I, Honma S, Hiroshige T. 1987. Activity rhythms in the circadian domain appear in suprachiasmatic nuclei lesioned rats given methamphetamine. *Physiol Behav*. 40(6):767–774.
74 Fujii H, *et al*. 2007. Methamphetamine-induced hyperactivity and behavioral sensitization in PACAP deficient mice. *Peptides*. 28(9): 1674–1679.
75 Salahpour A, *et al*. 2008. Increased amphetamine-induced hyperactivity and reward in mice overexpressing the dopamine transporter. *Proc Natl Acad Sci U S A*. 105(11):4405–4410.
76 Honma S, Kanematsu N, Honma K-I. 1992. Entrainment of methamphetamine-induced locomotor activity rhythm to feeding cycles in SCN-lesioned rats. *Physiol Behav*. 52(5):843–850.
77 Ono D, Honma S, Honma K-I. 2013. Postnatal constant light compensates Cryptochrome1 and 2 double deficiency for disruption of circadian behavioral rhythms in mice under constant dark. *PLoS One*. 8(11):e80615.
78 Putker M, *et al*. 2021. CRYPTOCHROMES confer robustness, not rhythmicity, to circadian timekeeping. *EMBO J*. 40(7):e106745.
79 Masubuchi S, Honma S, Abe H, Namihira M, Honma K-I. 2007. Methamphetamine induces circadian oscillation in the brain

outside the suprachiasmatic nucleus in rats. *Sleep Biol Rhythms*. 5(2):132–140.
80 Wever RA. *The circadian system of man: results of experiments under temporal isolation* Springer Science & Business Media, 1979.
81 Honma K, Hashimoto S, Natsubori A, Masubuchi S, Honma S. 2013. Sleep-wake cycles in humans. *Indian J Sleep Med*. 8(2):51–57.
82 Tang Q, Assali DR, Güler AD, Steele AD. 2022. Dopamine systems and biological rhythms: let's get a move on. *Front Integr Neurosci*. 16:957193.
83 Shaffer F, Ginsberg JP. 2017. An overview of heart rate variability metrics and norms. *Front Public Health*. 5:258.
84 Gehrman P, *et al*. 2005. The relationship between dementia severity and rest/activity circadian rhythms. *Neuropsychiatr Dis Treat*. 1(2):155–163.
85 Wang XS, Armstrong MEG, Cairns BJ, Key TJ, Travis RC. 2011. Shift work and chronic disease: the epidemiological evidence. *Occup Med*. 61(2):78–89.
86 Ashton A, Jagannath A. 2020. Disrupted sleep and circadian rhythms in schizophrenia and their interaction with dopamine signaling. *Front Neurosci*. 14:636.
87 Kondratov RV, Kondratova AA, Gorbacheva VY, Vykhovanets OV, Antoch MP. 2006. Early aging and age-related pathologies in mice deficient in BMAL1, the core component of the circadian clock. *Genes Dev*. 20(14):1868–1873.
88 Yoo S-H, *et al*. 2004. PERIOD2:: LUCIFERASE real-time reporting of circadian dynamics reveals persistent circadian oscillations in mouse peripheral tissues. *Proc Natl Acad Sci U S A*. 101(15):5339–5346.
89 Pendergast JS, *et al*. 2013. High-fat diet acutely affects circadian organisation and eating behavior. *Eur J Neurosci*. 37(8):1350–1356.
90 Ehichioya DE, Taufique SKT, Farah S, Yamazaki S. 2023. A time memory engram embedded in a light-entrainable circadian clock. *Curr Biol*. 33(23):5233–5239.
91 Bračič M, Stefanovska A. 1998. Wavelet-based analysis of human blood-flow dynamics. *Bull Math Biol*. 60(5):919–935.
92 Lancaster G, Iatsenko D, Pidde A, Ticcinelli V, Stefanovska A. 2018. Surrogate data for hypothesis testing of physical systems. *Phys Rep*. 748(4):1–60.
93 Jamšek J, Stefanovska A, McClintock PVE. 2007. Wavelet bispectral analysis for the study of interactions among oscillators whose basic frequencies are significantly time variable. *Phys Rev E*. 76(4):046221.
94 Paluš M, Vejmelka M. 2007. Directionality of coupling from bivariate time series: how to avoid false causalities and missed connections. *Phys Rev E*. 75(5):056211.
95 Iatsenko D, *et al*. Multiscale Oscillatory Dynamics Analysis (MODA) Toolbox. [accessed 2025 Feb 25] https://github.com/luphysics/MODA.